Article

Tailoring Vanadium-Based Magnetic Catalyst by In Situ Encapsulation of Tungsten Disulfide and Applications in Abatement of Multiple Pollutants

Suryyia Manzoor, Khalid Aziz, Hina Raza, Shamaila Manzoor, Muhammad Imran Khan, Asma Naz, Abdallah Shanableh, Alsamani A M Salih, and Noureddine Elboughdiri*

Cite This: *ACS Omega* 2023, 8, 48966−48974

Read Online

ACCESS | Metrics & More | Article Recommendations | SI Supporting Information

ABSTRACT: A magnetic nanocomposite of tungsten and vanadium was employed as a catalyst for the mitigation of water contaminants, including a carcinogenic dye (Congo red, CR), a widely used pesticide (glyphosate), and the bacterial strain *Escherichia coli*. Additionally, it was subjected to several characterization techniques. X-ray diffraction spectroscopy examination validated the synthesized nanoparticles' crystalline nature, and scanning electron microscopy and energy-dispersive X-ray analysis were employed to examine the morphology and elemental composition of the catalyst. The use of thermogravimetric analysis enabled the elaboration of the thermal behavior of tungsten sulfide−vanadium decorated with Fe_2O_3 nanoparticles. The experiments were conducted under visible light conditions. The

highest levels of photodegradation of 96.24 ± 2.5% for CR and 98 ± 1.8% for glyphosate were observed following a 180 min exposure to visible light at pH values of 6 and 8, respectively. The quantum yields for CR and Gly were calculated to be 9.2×10^{-3} and 4.9×10^{-4} molecules $photon^{-1}$, respectively. The findings from the scavenger analysis suggest the involvement of hydroxyl radicals in the degradation mechanism. The study evaluated the inhibition of *E. coli* growth when exposed to a concentration of 0.1 g/10 mL of the photocatalyst, utilizing a 1 mL sample of the bacterial strain. The successful elimination of CR and glyphosate from water-based solutions, along with the subsequent antibacterial experiments, has substantiated the efficacy of the photocatalyst in the field of environmental remediation.
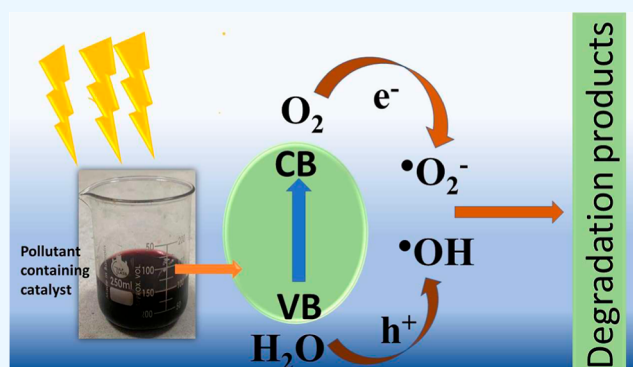
1. INTRODUCTION

In the current period of limited water resources, the unregulated release of contaminants by diverse industrial sectors, coupled with the discharge of inadequately treated or untreated effluents into aquatic ecosystems, poses a significant threat.[1,2] A notable proportion of these contaminants exhibit toxicity and resistance to degradation, leading to their tendency to accumulate in biological systems. Contaminants infiltrate the human system via the food chain, persisting and potentially resulting in the development of malignant tumors, given that numerous contaminants possess carcinogenic properties.[3] Water sources are often contaminated with a variety of organic and inorganic dyes, which are introduced as effluents.[4] Dyes serve as pigments employed in various sectors such as textiles, paint, photography, etc.[5] The adverse effects observed in water systems can be mostly linked to the structure and origin of dyes, notwithstanding their significant utility.[6−8] During the dyeing process, there is a possibility of an inadequate fixation of colors onto the substrate. As a consequence of this, the dyes are released into the environment, resulting in significant environmental ramifications.[9] The

decomposition of the anionic diazo Congo red (CR) presents significant challenges due to its intricate aromatic structures and the presence of physiochemical, thermoelectric, and electromagnetic stability.[10] Because of its toxic properties, this substance has the potential to act as a carcinogen and a mutagen for both humans and aquatic organisms. Adsorption has remained an appealing technique for the dye's removal, yet it has faced prominent challenges.[11−13] For example, firstly, the regeneration of the adsorbent requires some organic solvent; second, the desorbed dye needs further treatment to reduce its carcinogenic effects. The photocatalytic degradation is thus being opted as one of the prime techniques in combating the pollution caused by CR. Zinc oxide, the zinc oxide/copper
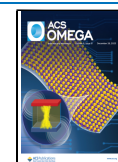
composite, cobalt molybdate, etc. have been used previously to degrade the dye presenting a degradation between 94 and 96%.[14,15] Various microorganisms found in water can lead to numerous outbreaks such as diarrhea and gastrointestinal illnesses.

Another category of organic substances that elicit detrimental impacts on aquatic organisms is pesticides, which are utilized to mitigate the damage caused by pests, insects, and undesirable vegetation to agricultural products.[16,17] Glyphosate (Gly) is a herbicide belonging to the organophosphate group.[18] It is a white crystalline solid and is recognized as the most extensively utilized pesticide globally for weed control, particularly targeting broad-leaf weeds.[19] Given the constraints associated with current approaches, it is imperative to develop proactive methodologies that can yield optimal outcomes in the degradation of persistent effluents into environmentally benign byproducts, such as water and carbon dioxide.

Owing to the challenges faced by conventional techniques, nanotechnology can help mitigate water problems. There is enormous scope for nanoparticles to be used in the treatment of wastewater.[20] The morphology, functional features, and antibacterial aspects, in addition to their particle size, contribute to the implementation of metal oxide nanoparticles. Recently, nanotechnology, due to its unique characteristics and features, has gained great attention for environmental remediation and sustainable energy production.[21,22] The photocatalysis technique is employed as an efficient method for the mineralization of deleterious organic compounds, the degradation of hazardous inorganic materials, the disinfection of microbial agents, and the inactivation of bacteria.[23]

Environmental remediation is achieved by photocatalysis, which involves the degradation of toxic pollutants into nonhazardous materials. For the promotion of photocatalysis and the transformation of solar energy, the surface of the metal oxide should be directly exposed to light so that photoelectrons and holes are generated and hold the whole reaction efficiently. Photocatalysis provides renewable energy resources and environmental remediation without causing any threats to the ecosystem as most of the degradation products are nonhazardous.[24] For example, in the case of glyphosate degradation, an oyster shell loaded with the cerium codoped nitrogen and titanium oxide photocatalyst was designed by Zhang et al. to mitigate its concentration, and they succeeded in achieving a percentage degradation of approximately 80%.[25] Due to their distinctive nature, transition metals are also widely used to control bacterial growth and environmental remediation. The size of a pore cell is greater than that of metal ions, so ions cannot cross the cell membrane but change the path with a lower inhibition rate using nanoparticles. The death of pathogenic bacteria can be caused by metal or metal oxide nanoparticles that penetrate the cell membrane.

To the best of the researcher's knowledge, the literature review revealed that there has not been any research on the synthesis of a tungsten−vanadium-based magnetic photocatalyst and its applications in the degradation of pollutants. WS_2 is viewed as a viable contender for the abatement of polluted water due to its decreased band gap and superior charge separation.[26] Tungsten disulfide is an intriguing stratified semiconductor intended as a material for absorption in photocatalysis because of its resilience and minimal toxic effects. S−W−S slabs are piled to create the stratified material known as tungsten disulfide.[27] Although the stacked S−W−S

slabs have minimal intermolecular van der Waals interactions connecting them, the slabs' hexagonally organized sulfur and tungsten atoms have a very strong bonding between them.[28−30] Through its superior conduction qualities and synergistic impact, vanadium can significantly increase photocatalytic activity by introducing it to the surface of tungsten sulfide. Fe_2O_3 has drawn interest in the domains of nanotechnology due to its special properties such as superparamagnetic nature, substantial saturation fields, and additional anisotropic contributions, which result from the effect of a small and huge surface area.[31] By reducing the aggregation of the heterostructure, the addition of nontoxic, inexpensive, and easily recoverable Fe_2O_3 can improve the photocatalytic activity.[32] Therefore, the current study involves the coprecipitation approach to prepare tungsten sulfide−vanadium decorated with Fe_2O_3 nanoparticles (WV-MNPs) for the robust abatement of common water pollutants. The WV-MNPs were used for the antimicrobial activity of the *Escherichia coli* bacterial strain and to find out the inevitable photodegradation of CR as well as glyphosate. In terms of performance, the newly designed photocatalyst outperformed various previously reported catalysts applied for the degradation of targeted pollutants.[25,33,34]

2. EXPERIMENTAL SECTION

2.1. Reagents. The chemicals used were all of analytical and biotechnology grade, and they were purchased from Sigma-Aldrich (Germany), including tungsten sulfide (WS_2, 99.99%), ammonium metavanadate (99.9%), ferrous sulfate ($FeSO_4 \cdot 7H_2O$, 99.0%), ferric acetate (99%), hydrochloric acid (HCl, 99.90%), sodium hydroxide (NaOH, 97%), and ethanol (C_2H_5OH, 99%). The following ingredients were purchased from Merck: nutrient broth (Lab-Lemco powder, yeast extract + peptone + NaCl, 98%), sodium chloride (NaCl, 99.99%), benzylpenicillin ($C_{16}H_{18}N_2O_4S$, 100%), amoxicillin ($C_{16}H_{19}N_3O_5S$, 100%), iodine crystals (I_2, 99.80%), and potassium iodate (KIO_3, 98. Deionized (DI) water was used during the whole research project and was filtered using the Milli-Q Plus method (Millipore, Bedford, MA, USA).

2.2. Synthesis of the WV-MNPs Photocatalyst. For the synthesis of the photocatalyst, 0.1 g of tungsten sulfide was suspended in DI water (50 mL) through ultrasonication. In the next step, solutions of 0.1 M ferrous sulfate, 0.1 M ferric acetate, and 0.1 M ammonium metavanadate were prepared. The three solutions were mixed and stirred at 70 °C for 5 min and introduced into the tungsten sulfide suspension. The sonication was continued, and the pH was adjusted to around 11−12 by adding 1 M NH_4OH dropwise. The resultant product was centrifuged and washed with HCl followed by DI water until the pH turned neutral. Then, the resultant product was thereafter placed in a crucible and subjected to heating within a furnace at 550 °C for 2.5 h. The obtained product was our required tungsten−vanadium magnetic photocatalyst (WV-MNPs).

2.3. Characterization Techniques. A Nova nano SEM-450 coupled with an energy-dispersive X-ray spectroscopy (EDX) device was used to record the scanning electron microscopy (SEM) images and EDX patterns of WV-MNPs. An XRD-Shamidzu-6100 was used to record the X-ray diffraction (XRD) pattern of WV-MNPs using Cu Kα radiation (λ = 1.5405 Å) for 5−90°. The surface area occupied by solid objects was calculated via the iodine value using various standards, especially iodine crystals and sodium
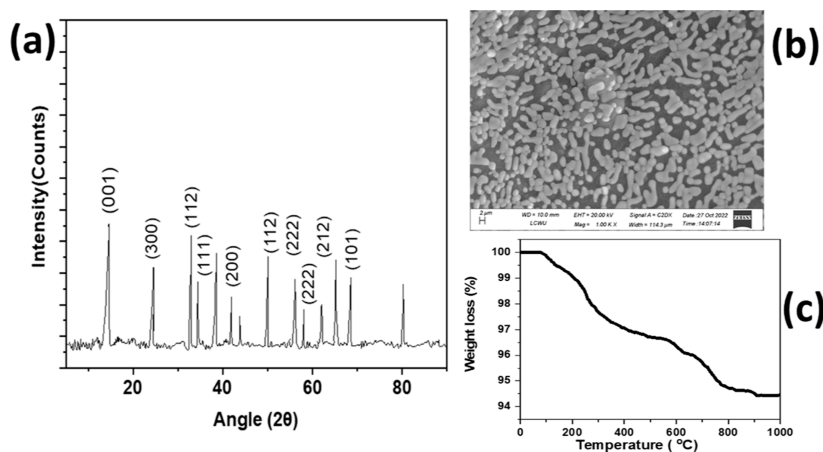
Figure 1. (a) XRD pattern of WV-MNPs, (b) SEM image of WV-MNPs, and (c) TGA graph of WV-MNPs representing the degradation behavior.

thiosulfate. The bonding nature was confirmed by a Raman Renishaw-6150 using a laser beam of 633 nm. The thermal nature of the WV-MNPs was investigated by a Netzsch STA-449 F1 at 1000 °C. Electron spin resonance (ESR) for trapping experiments was investigated by an EPR-Bruker-E580, using dimethyl pyrroline oxide (DMPO) for hydroxyl and super-oxide quenching, while a TEMPO adduct (tetramethylpiperidin-1-yl, oxyl) was used for hole trapping.

2.4. Photodegradation of Dyes and Pesticides. The photocatalytic performance of WV-MNPs for effluent removal was investigated in a closed black wooden box containing a visible bulb (Philip 500 W) as a visible light source. This closed photoreactor was used to inhibit any scattering of light by the reflection of incident light in order to optimize the quantity of photons emitted by the photocatalyst for the degradation of dyes and pesticides. For the photocatalytic study, first, the stock solution of each pollutant was prepared. After the mixture was stirred in the dark for 20 min, a 100 mL solution was obtained from the stock solution. The initial absorbance before irradiation with light was measured and denoted as A_0. Then, a 500 W Phillips light source was activated to verify the photocatalytic degradation of the CR and glyphosate (Gly) solutions in the presence of the photocatalyst with constant stirring. The distance was 7 cm between the liquid level and the light source, and 76.5 cm^2 was the total brightly lit portion of the photoreactor. Then, after every 20 min of stirring, 5 mL of the solution was centrifuged, and the absorbance was noted at different time intervals. The absorbances of CR and Gly were observed at 498 and 260 nm, respectively (A_t), by using a UV–vis spectrophotometer, and the percentage photodegradation was determined by the given formula

$$\% \text{ photodegradation} = A_0 - A_t / A_0 \times 100 \qquad (1)$$

Four parameters, such as the WV-MNPs dosage, pH, CR/Gly dosage, and contact time, were evaluated to find the optimum conditions for CR/Gly degradation.[35] The point zero charge (PZC) of WV-MNPs was calculated by adding 0.1 g of the photocatalyst into DI water to form a 1 L solution. 1 M NH_4OH and 1 M HNO_3 were used to adjust the pH from 2 to 12. After shaking the pH solutions overnight, a change in pH was observed, and the PZC was calculated.

2.5. Antibacterial Activity. An *E. coli* strain, classified as Gram-negative, was cultured within a biosafety cabinet (specifically, an RBSCA Class-II Type A2 model manufactured

by Robus Technologies). This was accomplished by streaking the strain from a well-preserved glycerol stock culture onto an LB–Agar plate. The plates were incubated at 28 °C in a tabletop incubator for 12 h. A single colony was selected from the plate in order to inoculate 5.0 mL of LB broth medium within a culture tube. The sample was thereafter placed in a shaking incubator (Wis-20, Witeg, Germany) and incubated at 28 °C for 2 h. Four flasks were then taken and labeled as A1, B1, C1, and D1. A1 was considered as the negative control and contained only 1.0 mL of bacterial suspension in 10 mL of doubly distilled water. In flask B, the suspension material was prepared by mixing 1.0 mL of a recently cultured *E. coli* strain with 0.1 g of NaCl and 0.01 g of the photocatalyst in 10 mL of sterile double distilled water.[36] The flasks C1 and D1 contained 50 g of amoxicillin and 50 g of ampicillin along with the bacterial suspension as positive controls.

2.6. Real Sample Analysis. In order to determine the efficiency of the catalyst to degrade the pollutants in real samples, a canal water sample was collected from the vicinity and filtered with Whatman filter paper (grade 1) followed by filtration through a 0.45 μm syringe filter (Whatman Spartan). 10 mL of the filtered sample was taken separately in each flask and spiked with 10 mL of 10 mg L^{-1} CR and Gly standard solutions. The optimum quantity of the catalyst dose was added to each, the pH was adjusted, and the sample was irradiated under visible light (500 W bulb) for 180 min. Percentage photodegradation was then calculated using eq 1 described in Section 2.4.

3. RESULTS AND DISCUSSION

3.1. X-ray Diffraction Studies. The crystallinity and particle size of WV-MNPs were analyzed by XRD. The XRD pattern of the photocatalyst is presented in Figure 1a. Uniformly phased hematite Fe_2O_3 showed characteristics peaks at 33, 42, 50, 55, and 62° with respective planes at (111), (200), (112), (222), and (212), fully matching the JCDP card number 892810. The polycrystalline nature of WS2 showed peaks at 14, 34, 58, and 68° corresponding to planes at (001), (112), (222), and (101), respectively, well matched with the JCDP file number 080237. The crystalline nature of vanadium showed peaks at 15 and 24° with *hkl* values (001) and (200), respectively, matched with the JDCP file number 311483. The Scherer equation determined that the average crystal size of WV-MNPs was 39 nm.

3.2. Surface Area and Morphological Analysis. The WV magnetic nanocomposites presented a high surface area, determined by the iodine value method followed by standardization of iodine (I_2) and sodium thiosulfate, which was 140 m^2/g.[36] With the help of eq 2, the surface area of the WV-MNPs was calculated.

$$\text{Surface area} = 253.8[\text{volume of iodine}(X_i - X_f)] \qquad (2)$$

Here, 253.8 eV is the surface area of 1 M iodine and X_i and X_f are the concentrations of iodine before and after adsorption, respectively.

The morphology of prepared WV-MNPs obtained by SEM is shown in Figure 1b. The study of the image presents the appearance of the photocatalyst as cylindrical rod-like structures. In order to confirm the incorporation of required elements into WV-MNPs, an EDX analysis was performed. All the constituent elements were observed in the EDX spectrum of the synthesized composite. In the spectrum, the atomic ratios of W, V, Fe, S, C, and O were 44.8, 7.7, 16.3, 11.0, 8.1, and 12.07%, respectively.

3.3. Thermogravimetric Analysis. The thermal behavior of WV-MNPs was investigated using a uniform heating rate of 15 °C min^{-1} to carry out the thermogravimetric analysis (TGA). Thermal analysis confirmed three zones of weight loss for WV-MNPs (Figure 1c). The 2% weight loss up to 300 °C may be attributed to the evaporation of any water residues present in the network structure. Around a 1.5% weight loss up to 600 °C may be assigned to the elimination of any oxide or sulfide residues in the WV-MNPs structure. After 600 °C, a weight loss of 2% may be due to slight damage to the network structure. Only a 5.5% weight loss after 1000 °C confirmed the higher thermal stability of WV-MNPs.

3.4. Optimization of Operational Parameters. The photocatalytic downgrading of CR and Gly was investigated to determine the catalytic activity of the WV-MNPs. The degradation profile was studied for four parameters: optimization of the catalyst dose, pH, contact time, and concentration of pollutants.

3.4.1. Photocatalyst Dose. To check the effectiveness of the photocatalyst, a 5 mg L^{-1} CR concentration was added to different amounts of WV-MNPs (20−160 mg), and absorption was investigated for 240 min. Results indicated that the maximum CR removal of 94% and glyphosate removal (96.5%) were achieved for 120 mg and 100 mg of WV-MNPs, respectively, after that, it became constant (Figure S1a). With increasing amounts of WV-MNPs, active sites increased, yielding enhanced photocatalytic removal of CR and glyphosate. After achieving equilibrium, photodegradation became constant, possibly due to the maximum effluent molecules' attachment to the active sites of WV-MNPs.[37]

3.4.2. pH Effect. The photocatalytic degradation of 10 mg L^{-1} CR and Gly solutions with 120 and 100 mg of WV-MNPs was investigated within the range of pH 2−12 in 180 min using 1 M HCl and 1 M NaOH. The graph in Figure S1c shows that the maximum CR degradation of 96.24% was achieved at pH 6, while 98% Gly degradation was achieved at pH 8. A decrease in the photodegradation percentage of CR and Gly in both acidic and basic conditions can be related to the surface charge of WV-MNPs. The PZC of WV-MNPs found by the pH drift method was 7.4 (Figure S1b). CR shows maximum protonation (positive nature) at pH 5.5 as its pK_a is in the range of 4.5−5.5. Below the PZC, the surface of WV-MNPs is predominantly positively charged, so with increasing acidity,

protonated effluent molecules and the positively charged surface of WV-MNPs will show a decrease in degradation due to the same charge repulsion. When pH is increased from the PZC, the surface of WV-MNPs is negative, and effluent molecules are also present in the deprotonated form (negative nature). So, again, the same charge repulsion decreases degradation efficiency.[38]

3.4.3. Effect of Irradiation Time. For the optimization of time, a 10 mg pollutant solution with 120 and 100 mg doses of the composite for CR and Gly, respectively, was investigated for 4 h. The degradation results for CR and glyphosate at various time intervals by WV-MNPs are presented in Figure S1d. Results confirmed that maximum CR degradation (96.24%) and glyphosate degradation (98%) were achieved in 3 h and then became constant. Results predicted that swift degradation occurred initially as more than half of the pollutants degraded in just 1 h. This fast photodegradation may be due to the speedy production of reactive species and the presence of a maximum number of pollutant molecules in the degradation process. The movement of free electrons in WV-MNPs to higher energy levels results in hole creation at lower energy levels, causing the production of reactive species for CR and Gly degradation. After an optimum time, photodegradation became constant, which may possibly be due to the fact that almost all the pollutant molecules were converted to degradation products.[39]

3.4.4. Effect of CR Concentration. Varying concentrations of CR (10 to 60 mg L^{-1}) were prepared to optimize the suitable amount of CR and Gly degraded by the optimum amount of WV-MNPs in 180 min. A graph (Figure S1e) shows optimum CR and Gly degradation values at 10 mg L^{-1}, which were 96.24 and 98% respectively; after that, degradation started to decrease. Degradation efficiency was maximum at lower concentrations as all the molecules of CR and Gly were adsorbed on the active sites of WV-MNPs, indicating maximum interaction between the pollutant and WV-MNPs. As a fixed amount of WV-MNPs was used, after the optimized value, incoming pollutant molecules could not find the required number of active sites on the catalyst surface, resulting in a lowering of the degradation efficiency. This decrease in photocatalytic activity with increasing pollutant concentration can also be validated by Lambert's law as decreased path lengths of generated photons are observed with increasing dye concentration.[40]

3.4.5. Intensity of Visible Light. The irradiation of WV-MNPs with an illumination source is necessary to enable the production of reactive species such as holes, super oxides, and hydroxyl radicals. The intensity of the visible light source was changed from 100 to 500 W, and the photodegradation of CR and Gly was examined. According to the findings, both CR and Gly degraded more effectively as light intensity increased (Figure S1f). The more rapid generation of reactive species and a slower recombination mechanism with a higher light intensity may be responsible for the increase in degradation with increasing intensity.

3.4.6. Degradation of CR and Gly in a Real Water Sample. The photodegradation of CR and Gly in real water samples is crucial for practical execution. The results showed that compared to DI water (96.24% for CR and 98% for Gly in DI water), CR and Gly showed a noticeable drop in degradation efficiency (84.7% for CR and 86.5% for Gly) in canal water (Figure S1g). This modest decline might have been possible due to the presence of contaminants and

biological contents that make the matrix nature complex as compared to DI water.

3.5. Photocatalytic Degradation of CR and Glyphosate at Optimum Conditions. At optimized conditions, CR degradation spectra were recorded for 180 min by using 10 mg L^{-1} pollutant solution and 100 mg of WV-MNPs at pH 6, while Gly degradation was investigated for 120 mg of catalysts and 10 mg L^{-1} Gly solution at pH 8 for 180 min. The characteristic absorbance peaks of CR (498 nm) and Gly (260) decreased constantly with time, becoming almost flat after 180 min, confirming the degradation of CR and Gly. Absorbance results confirmed the maximum degradation of both the pollutants (Figure 2a,b) as no prominent peak of any pollutant was observed at a time scale of 180 min.
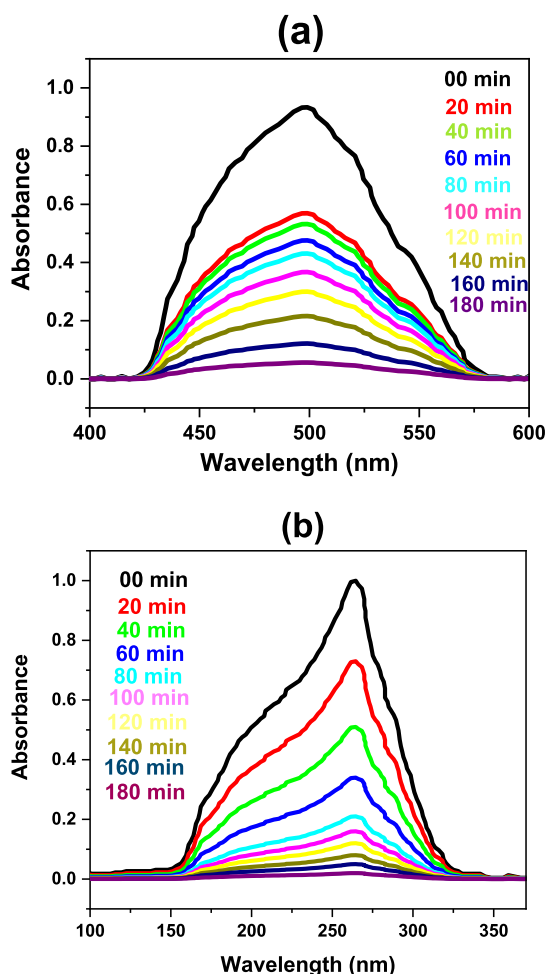

Figure 2. UV−vis absorption spectra of (a) CR and (b) glyphosate.

3.6. Kinetics Study. The Langmuir−Hinshelwood model was applied to investigate the kinetics of the photocatalytic degradation of CR and glyphosate by WV-MNPs. The adsorption of CR and glyphosate on the surface of WV-MNPs was used to predict the rate-determining step for heterogeneous photocatalysis.[41,42] Pseudo-first-, first-, and second-order kinetics were investigated using S1−S3 equations given in the Supporting Information file.

Comparison of the regression constant values predicted the best fitting of pseudo-first-order kinetics for CR and glyphosate degradation by WV-MNPs. (Figure 3a−c) Pseudo-first-order kinetics confirmed the fact that only the amount of CR and
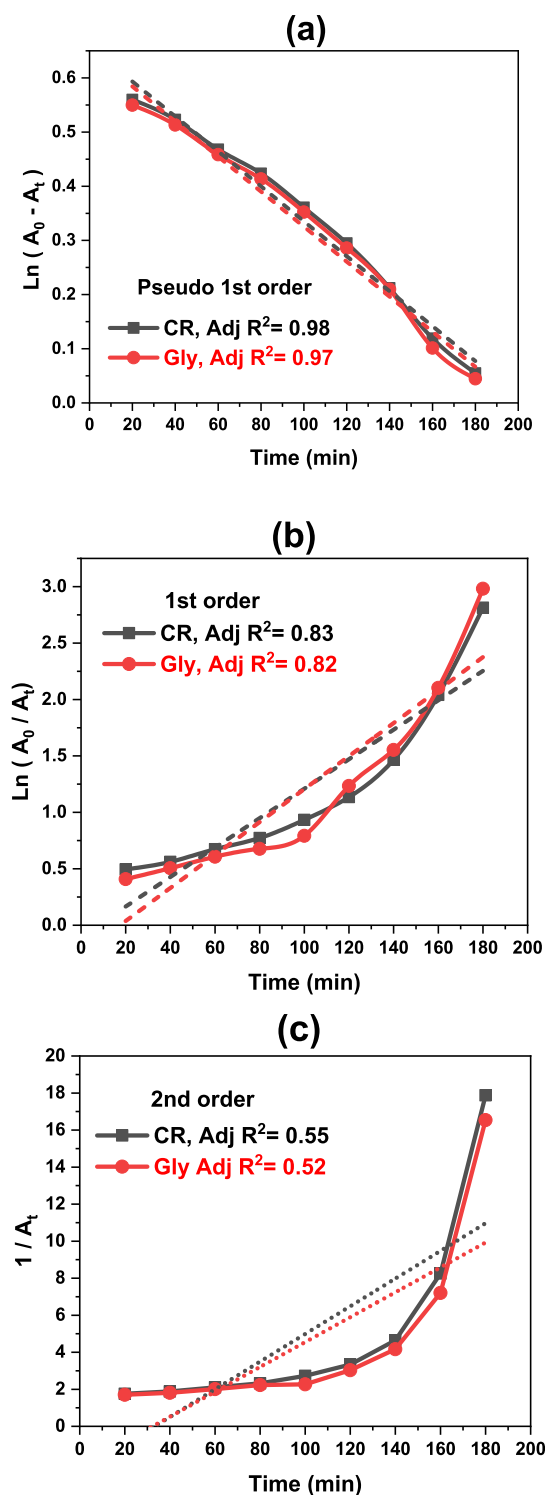

Figure 3. Linear fit and kinetics analysis for (a) pseudo-first-, (b) first-, and (c) second-order reactions.

glyphosate took part in predicting the rate of reaction as the amount of the photocatalyst was completely regenerated after the degradation process.

3.7. Possible Degradation Mechanism and Scavenger Analysis. On irradiation with photons, if a semiconducting material absorbs more energy than its band gap, excitation will produce holes (h$^+$) and electrons (e$^-$).[43] Shifting e$^-$ to the conduction band (CB) will result in the creation of an h$^+$ vacancy in the valence band.[44] A decreased recombination rate

of h^+ and e^- is responsible for the increased generation of reactive species for the photocatalytic abatement of effluents. The influence of individual reactive species on the photocatalytic performance of WV-MNPs was evaluated by their role in quenching the degradation efficiency of CR and Gly. Three common reactive species, hydroxyl radicals ($^\bullet OH$), h^+, and superoxide radicals ($^\bullet O_2^-$), were quenched by isopropyl alcohol (IPA), Na_2-EDTA, and benzoquinone (BQ), respectively. 2 mg of the scavenging agent, 10 mg of the pollutant, and 100 mg of the synthesized WV-MNPs were added to DI water to form a 1 L solution by maintaining the pH at 6, and photocatalytic performance was evaluated for 180 min, while 120 mg of the catalyst and pH 8 were used for glyphosate removal. Maximum quenching was noted for hydroxyl radicals as reactive species were trapped by IPA, and degradation efficiency dropped from 96 to 39% for CR, while glyphosate degradation decreased from 98 to 44%. Considerable quenching was observed for holes and superoxide radicals as degradation efficiency was considerably decreased for CR and glyphosate (Figure 4). The weaker quenching effect of holes
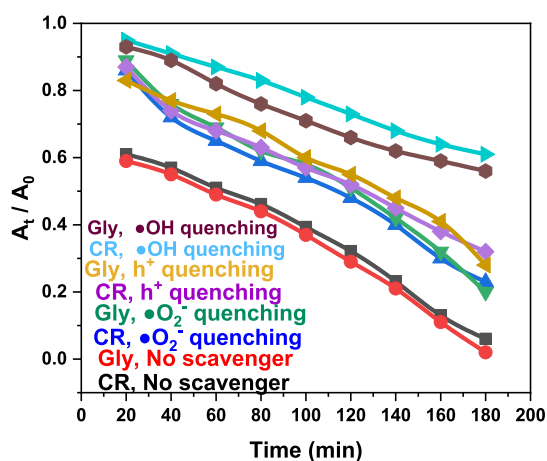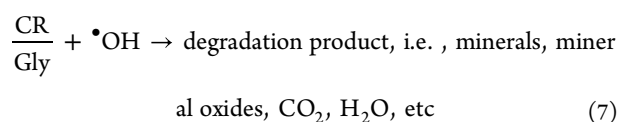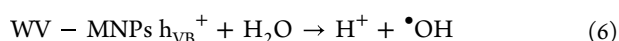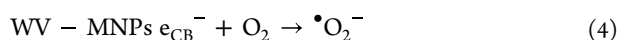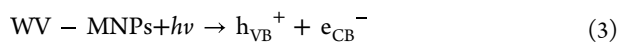

Figure 4. Role of scavengers in the photodegradation process.

and superoxide radicals than that of hydroxyl radicals may be due to their conversion into hydroxyl radicals.

$$WV - MNPs + h\nu \rightarrow h_{VB}^+ + e_{CB}^- \tag{3}$$

$$WV - MNPs\ e_{CB}^- + O_2 \rightarrow {}^\bullet O_2^- \tag{4}$$

$$2H^+ + {}^\bullet O_2^- \rightarrow 2^\bullet OH \tag{5}$$

$$WV - MNPs\ h_{VB}^+ + H_2O \rightarrow H^+ + {}^\bullet OH \tag{6}$$

$$\frac{CR}{Gly} + {}^\bullet OH \rightarrow \text{degradation product, i.e. , minerals, miner}$$

$$\text{al oxides, } CO_2, H_2O, \text{etc} \tag{7}$$

3.8. ESR Spectroscopic Analysis. To verify the outcomes of the scavenger test, the impact of different reactive species on the photodegradation of CR was further examined by ESR analysis. ESR analysis for CR absorption was used to examine the involvement of the most prevalent reactive species, including holes, hydroxyl radicals, and superoxide radicals, in the photodegradation process.[43] No signals were recorded in the absence of light because reactive species are active only when exposed to visible light. The hydroxyl radical adducts for

ESR investigation displayed maximum intensity during visible light irradiation (Figure 5). This increased intensity suggested a greater $^\bullet OH$ generation and improved $^\bullet OH$ stability, which resulted in the maximum photodegradation of CR.
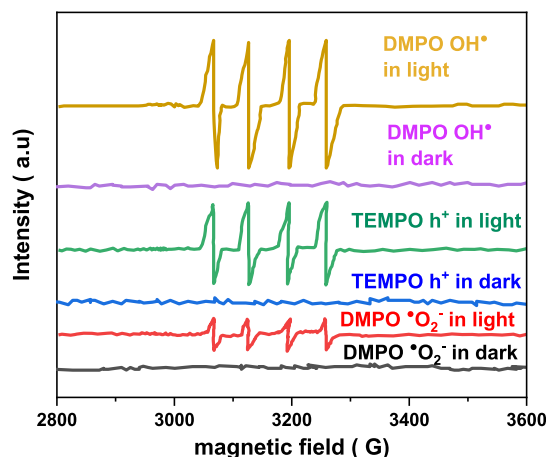

Figure 5. ESR spectra for various reactive species for CR and glyphosate degradation.

3.9. Fragmentation Process and Degradation Path. The incorporation of the electrospray ionization mass spectrometry (ESI-MS_ investigation to forecast potential fragmentation processes for CR and Gly helped further clarify the degradation path. ESI-MS spectra of CR and Gly were obtained before and during the degradation process. Prior to degradation, Gly showed a peak at about 169, while CR indicated peaks at 650, 571, and 492 (Figure S2a,b). CR displayed significant peaks at 633, 550, 469, 387, 308, and 220 nm during the degradation process (after 100 min), whereas Gly displayed notable peaks at 129, 115, 89, and 75 nm during degradation. The probable fragmentation path elaborating the m/z peaks of the spectra is shown in Figure S2c,d. Additionally, the existence of smaller peaks during degradation shows the fast conversion of unstable intermediates to degradation products.

3.10. Sustainability of WV-MNPs. Higher endurance of developed materials with improved catalytic performance is essential for practical application of nanoparticles for ecological restoration. For six cycles, the reusability of WV-MNPs for CR and Gly degradation was assessed. After each cycle, nanoparticles were centrifuged, rinsed with HCl and DI water, dried, and reused. Results showed that after six cycles of photodegradation, CR degradation marginally decreased from 96.24 to 88%, whereas glyphosate degradation slightly dropped from 98 to 90% (Figure S3a). The XRD spectrum of WV-MNPs after six cycles of CR and Gly degradation revealed the persistence of all the distinctive peaks of the material, indicating the structure's sustainability (Figure S3b). Furthermore, no additional XRD peaks were noticed after degradation, proving that the pollutant molecules were not chemically linked to the WV-MNPs and could be easily revitalized. The small decrease in degradation after six cycles of CR and Gly degradation may be related to surface roughness and blocking of some active sites.

3.11. Antimicrobial Activity of WV-MNPs. Among the four flasks, the one labeled as A1 presented the maximum bacterial growth (negative control). This culture's absorbance was the highest of all samples at 600 nm at 0.365, which caused

Table 1. Comparison of the Current Study (WV-MNPs) with the Previously Reported Literature

photocatalyst	pollutant	light source	catalyst dose mg L^{-1}	CR conc. mg L^{-1}	time min	CR % removal	number of photons produced	number of moles destructed	quantum yield (molecules photon^{-1})	refs
Fe$_2$O$_3$@CeO$_2$−ZrO$_2$	CR	300	4000	500	105	95	7.8×10^{24}	6.8×10^{-2}	5.2×10^{-3}	46
α-Fe$_2$O$_3$	CR	80	50	40	90	90	6.7×10^{24}	5.2×10^{-2}	4.6×10^{-3}	47
furnace slag Fe$_2$O$_3$	CR	40	400	6	100	99	6×10^{23}	8.5×10^{-3}	8.5×10^{-3}	48
green α-Fe$_2$O$_3$	CR	647	50	50	240	87	2.3×10^{25}	6.2×10^{-3}	1.6×10^{-4}	49
V$_2$O$_5$	CR	300	150	100	180	99	8.1×10^{24}	1.4×10^{-2}	1.1×10^{-3}	50
chitosan−V−Ti	CR	300	2000	1000	50	99	2.7×10^{24}	1.4×10^{-1}	3.1×10^{-2}	51
TiO$_2$−WO$_3$	CR	250	500	20	120	95	4.5×10^{24}	2.7×10^{-3}	3.6×10^{-4}	44
W doped TiO$_2$	CR	650	15	30	60	90	5.8×10^{24}	3.9×10^{-3}	4.1×10^{-4}	52
WS$_2$−WSe$_2$	CR	300	1000	30	60	92	2.7×10^{24}	1.3×10^{-2}	2.9×10^{-3}	53
WV-MNPs	CR	500	100	10	180	96	7.4×10^{24}	9.7×10^{-2}	9.2×10^{-3}	current study
C$_3$N$_4$−ZnWO$_4$	Gly	150	30	15	180	99	7.4×10^{24}	4.1×10^{-2}	5.9×10^{-4}	54
W doped ZnO	Gly	8	150	20	180	74	2.3×10^{24}	3.9×10^{-2}	6.5×10^{-3}	33
BiVO$_4$	Gly	125	500	10	180	55	1.1×10^{24}	3.4×10^{-2}	2.1×10^{-4}	34
WV-MNPs	Gly	500	120	10	180	98	9.6×10^{25}	5.8×10^{-2}	4.9×10^{-4}	current study

the color to change to milky. 50 g of amoxicillin and 50 g of ampicillin, used as positive controls, respectively, resulted in minimal bacterial growth measurements of 0.190 and 0.280. In flasks C1 and D1, it was shown that these antibiotics significantly inhibited bacterial growth (Figure S4). The use of WV-MNPs in the treatment showed their capacity to greatly reduce bacterial growth. This bacterial culture's absorbance, which was tested at 0.295 in flask B1, was lower than that of the negative control, which was recorded at 0.365 in flask A1. It was evident that the flask containing the WV-MNPs was more effective than the negative control at reducing the rate of bacterial growth. Figure S3 shows the relative activity order in accordance with the following absorbance observations

C1 > D1 > B1 > A1

The inclusion or coating of WV-MNPs on the targeted substrate and the destruction of the biofilm (i.e., *E. coli* strains) are the causes of the decrease in colonized bacteria with the use of metal nanoparticles. The several components of a general bacteria (*E. coli*) (cell wall, cytoplasm, etc.) are the targets of the antimicrobial process mediated by nanoparticle interactions. The metal toxicity of NPs expectedly damages the cell wall and electron transport chain. This causes the formation of ROS (reactive oxygen species), which further disturb the proton absorption mechanism as well as interact with the RNA. All these processes mark the inhibition of protein synthesis and nucleic acid replication, resulting in cell death. The population of bacteria thus decreases as a result.[45]

3.12. Comparative Analysis. Nanomaterials of various metals have been reported for CR and Gly degradation. According to the literature survey, vanadium- and tungsten-based materials have been very rarely reported for photocatalytic degradation of CR and Gly. In the current study, WV-MNPs were prepared for CR and glyphosate degradation and showed promising results for photocatalytic activity with the production of a higher number of photons and an increased quantum yield. A comparison between the current study and previously reported iron oxide-, tungsten-, and vanadium-based nanoparticles has been presented in Table 1.

4. CONCLUSIONS

The interpretation enables us to observe the effective synthesis of WV magnetic nanoparticles for environmental remediation. The WV-MNPs were characterized by an iodine value for the surface that was 152.28 m^2/g, and EDX showed that the concentrations of tungsten, vanadium, and iron were 44.81, 7.7, and 16.31%, respectively. SEM images showed spherical sheets, an amorphous distribution, and agglomeration on them. The XRD pattern further confirmed the efficient synthesis of functionalized nanoparticles. The research reveals that wastewater, polluted with carcinogenic dyes, pesticides, and microbes, can be purified by WV magnetic nanoparticles. Four different parameters were performed for the degradation of CR and glyphosate, along with maximum results, such as the optimized parameters that confirmed 96.24 and 98% degradation of CR and glyphosate, respectively, in 180 min. The inhibition of bacteria was observed against Gram-negative bacillus *E. coli* by using antibiotics (benzylpenicillin and amoxicillin) and WV-MNPs, and the best result was shown by amoxicillin, then benzylpenicillin, and then the WV magnetite nanocomposite.

■ ASSOCIATED CONTENT

Ⓢ Supporting Information

The Supporting Information is available free of charge at https://pubs.acs.org/doi/10.1021/acsomega.3c06580.

> Various kinetics equations; effect of catalyst dosage, pH, CR/Gly amount, irradiation time, visible light power, and canal water on photodegradation of CR and Gly; ESI-MS degradation spectrum and possible fragmentation path for CR and glyphosate; reusability of WV-MNPs for photodegradation of CR and glyphosate, XRD of WV-MNPs before and after six cycle of CR and Gly degradation; and bar graph for antibacterial activity (PDF)

■ AUTHOR INFORMATION

Corresponding Author

Noureddine Elboughdiri − *Chemical Engineering Department, College of Engineering, University of Ha'il, Ha'il 81441, Saudi Arabia; Chemical Engineering Process*

Department, National School of Engineers Gabes, University of Gabes, Gabes 6029, Tunisia; ● orcid.org/0000-0003-2923-3062; Email: ghilaninouri@yahoo.fr

Authors

Suryyia Manzoor − *Institute of Chemical Sciences, Bahauddin Zakariya University, Multan 60000, Pakistan*

Khalid Aziz − *Institute of Chemical Sciences, Bahauddin Zakariya University, Multan 60000, Pakistan*

Hina Raza − *Faculty of Pharmacy, Bahauddin Zakariya Unviersity, Multan 60000, Pakistan*

Shamaila Manzoor − *Department of Experimental Physics, Faculty of Mathematics, Physics and Informatics, Comenius University, Bratislava 842 48, Slovakia*

Muhammad Imran Khan − *Research Institute of Sciences and Engineering (RISE), University of Sharjah, Sharjah 27272, United Arab Emirates*

Asma Naz − *Institute of Chemical Sciences, Bahauddin Zakariya University, Multan 60000, Pakistan*

Abdallah Shanableh − *Research Institute of Sciences and Engineering (RISE), University of Sharjah, Sharjah 27272, United Arab Emirates*

Alsamani A M Salih − *Chemical Engineering Department, College of Engineering, University of Ha'il, Ha'il 81441, Saudi Arabia; Department of Chemical Engineering, Faculty of Engineering, Al Neelain University, Khartoum 12702, Sudan*

Complete contact information is available at:
https://pubs.acs.org/10.1021/acsomega.3c06580

Notes

The authors declare no competing financial interest.

■ REFERENCES

(1) Zhang, L.; Jiang, Y.; Ding, Y.; Povey, M.; York, D. Investigation into the antibacterial behaviour of suspensions of ZnO nanoparticles (ZnO nanofluids). *J. Nanopart. Res.* **2007**, *9* (3), 479−489.

(2) Tariq, A.; Mushtaq, A. Untreated wastewater reasons and causes: a review of most affected areas and cities. *Int. J. Chem. Biochem. Sci.* **2023**, *23*, 121−143.

(3) Costa, M.; Simmons-Hansen, J.; Bedrossian, C. W. M.; Bonura, J.; Caprioli, R. M. Phagocytosis, cellular distribution, and carcinogenic activity of particulate nickel compounds in tissue culture. *Cancer Res.* **1981**, *41* (7), 2868−2876.

(4) Ansari, S. A.; Parveen, N.; Alsulaim, G. M.; Ansari, A. A.; Alsharif, S. A.; Alnahdi, K. M.; Alali, H. A.; Reddy, V. Emerging NiO-rGO Nanohybrids for Antibiotic Pollutant Degradation Under Visible-Light Irradiation. *Surf. Interfaces* **2023**, *40*, 103078.

(5) Ansari, S. A.; Kumar, R.; Barakat, M.; Cho, M. H. Simple and sustainable route for large scale fabrication of few layered molybdenum disulfide sheets towards superior adsorption of the hazardous organic pollutant. *J. Mater. Sci.: Mater. Electron.* **2018**, *29*, 7792−7800.

(6) Jones, K.; Sharpe, G. Ni2+ blocks the Ca2+ influx in human keratinocytes following a rise in extracellular Ca2+. *Exp. Cell Res.* **1994**, *212* (2), 409−413.

(7) Robison, S. H.; Cantoni, O.; Heck, J. D.; Costa, M. Soluble and insoluble nickel compounds induce DNA repair synthesis in cultured mammalian cells. *Cancer Lett.* **1983**, *17* (3), 273−279.

(8) Oller, A. R. Respiratory carcinogenicity assessment of soluble nickel compounds. *Environ. Health Perspect.* **2002**, *110*, 841−844.

(9) Mansoori, G. A.; Fauzi Soelaiman, T. A. Nanotechnology—an introduction for the standards community. *J. ASTM Int.* **2005**, *2* (6), JAI13110.

(10) Kumar, R.; Ansari, S. A.; Barakat, M.; Aljaafari, A.; Cho, M. H. A polyaniline@ MoS 2-based organic-inorganic nanohybrid for the removal of Congo red: adsorption kinetic, thermodynamic and isotherm studies. *New J. Chem.* **2018**, *42* (23), 18802−18809.

(11) Wang, H.; Luo, W.; Guo, R.; Li, D.; Xue, B. Effective adsorption of Congo red dye by magnetic chitosan prepared by solvent-free ball milling. *Mater. Chem. Phys.* **2022**, *292*, 126857.

(12) Arab, C.; El Kurdi, R.; Patra, D. Zinc curcumin oxide nanoparticles for enhanced adsorption of Congo red: kinetics and adsorption isotherms study. *Mater. Today Chem.* **2022**, *23*, 100701.

(13) Jin, Y.; Li, Y.; Du, Q.; Chen, B.; Chen, K.; Zhang, Y.; Wang, M.; Sun, Y.; Zhao, S.; Jing, Z.; et al. Efficient adsorption of Congo red by MIL-53 (Fe)/chitosan composite hydrogel spheres. *Microporous Mesoporous Mater.* **2023**, *348*, 112404.

(14) Hitkari, G.; Chowdhary, P.; Kumar, V.; Singh, S.; Motghare, A. Potential of Copper-Zinc Oxide nanocomposite for photocatalytic degradation of congo red dye. *Clean. Chem. Eng.* **2022**, *1*, 100003.

(15) Zhou, H.; Qiu, Y.; Yang, C.; Zang, J.; Song, Z.; Yang, T.; Li, J.; Fan, Y.; Dang, F.; Wang, W. Efficient Degradation of Congo Red in Water by UV-Vis Driven CoMoO4/PDS Photo-Fenton System. *Molecules* **2022**, *27* (24), 8642.

(16) Hayat, M.; Manzoor, S.; Raza, H.; Khan, M. I.; Shanableh, A.; Sajid, M.; Almutairi, T. M.; Luque, R. Molecularly imprinted ormosil as a sorbent for targeted dispersive solid phase micro extraction of pyriproxyfen from strawberry samples. *Chemosphere* **2023**, *320*, 137835.

(17) Hayat, M.; Manzoor, S.; Raza, N.; Abbas, A.; Khan, M. I.; Elboughdiri, N.; Naseem, K.; Shanableh, A.; Elbadry, A. M.; Al Arni, S.; et al. Molecularly Imprinted Polymeric Sorbent for Targeted Dispersive Solid-Phase Microextraction of Fipronil from Milk Samples. *ACS Omega* **2022**, *7* (45), 41437−41448.

(18) Martins-Gomes, C.; Silva, T. L.; Andreani, T.; Silva, A. M. Glyphosate vs. glyphosate-based herbicides exposure: A review on their toxicity. *J. Xenobiot.* **2022**, *12* (1), 21−40.

(19) Aziz, K.; Naz, A.; Manzoor, S.; Khan, M. I.; Shanableh, A.; Fernandez Garcia, J. Visible Light Photodegradation of Glyphosate and Methylene Blue Using Defect-Modified Graphitic Carbon Nitride Decorated with Ag/TiO2. *Catalysts* **2023**, *13* (7), 1087.

(20) Linsebigler, A. L.; Lu, G.; Yates, J. T., Jr. Photocatalysis on TiO2 surfaces: principles, mechanisms, and selected results. *Chem. Rev.* **1995**, *95* (3), 735−758.

(21) Corsi, I.; Venditti, I.; Trotta, F.; Punta, C. Environmental safety of nanotechnologies: The eco-design of manufactured nanomaterials for environmental remediation. *Sci. Total Environ.* **2023**, *864*, 161181.

(22) Govarthanan, M.; Manikandan, S.; Subbaiya, R.; Krishnan, R. Y.; Srinivasan, S.; Karmegam, N.; Kim, W. Emerging trends and nanotechnology advances for sustainable biogas production from lignocellulosic waste biomass: a critical review. *Fuel* **2022**, *312*, 122928.

(23) Sakkas, V. A.; Islam, M. A.; Stalikas, C.; Albanis, T. A. Photocatalytic degradation using design of experiments: a review and example of the Congo red degradation. *J. Hazard. Mater.* **2010**, *175* (1−3), 33−44.

(24) Liu, S.-Q. Magnetic semiconductor nano-photocatalysts for the degradation of organic pollutants. *Environ. Chem. Lett.* **2012**, *10* (3), 209−216.

(25) Zhang, W.; You, Q.; Shu, J.; Wang, A.; Lin, H.; Yan, X. Photocatalytic degradation of glyphosate using Ce/N co-doped TiO2 with oyster shell powder as carrier under the simulated fluorescent lamp. *Front. Environ. Sci.* **2023**, *11*, 61.

(26) Zhou, K.; Yu, H.; Li, Q.; liang, D.; Luo, J.; Yu, Y.; Zhang, C.; Sun, Y.; Wu, C.; Cheng, Z. Application of phosphomolybdate/ tungsten disulfide composites in the adsorption and photocatalytic

degradation of dyeing wastewater. *Sep. Purif. Technol.* **2024**, *330*, 125431.

(27) Wang, E.; Ding, S.; Zhang, J.; Yu, L.; Zhang, Y.; Jiang, C.; Yang, G.-S. PW11Co/Ag3PO4/WS2 ternary composites with enhanced photocatalytic performance for the degradation of organic pollutants under visible light. *Mater. Lett.* **2023**, *351*, 135048.

(28) Jamal, F.; Rafique, A.; Moeen, S.; Haider, J.; Nabgan, W.; Haider, A.; Imran, M.; Nazir, G.; Alhassan, M.; Ikram, M.; et al. Review of Metal Sulfide Nanostructures and their Applications. *ACS Appl. Nano Mater.* **2023**, *6* (9), 7077−7106.

(29) Tahir, M. Vanadium Carbide (V_2CT_x) MXene-Supported Exfoliated g-C_3N_4 with the Role of Hole Scavenger as a Rapid Electron Transfer Channel for Enhancing Photocatalytic CO_2 Reduction to CO and CH_4. *Energy Fuels* **2023**, *37* (14), 10615−10630.

(30) Feng, X.; Xian, D.; Fu, J.; Luo, R.; Wang, W.; Zheng, Y.; He, Q.; Ouyang, Z.; Fang, S.; Zhang, W.; et al. Four-armed host-defense peptidomimetics-augmented vanadium carbide MXene-based micro-needle array for efficient photo-excited bacteria-killing. *Chem. Eng. J.* **2023**, *456*, 141121.

(31) Inam, H.; Fatima, U.; Shahid, S.; Mansoor, S.; Yasin, A.; Javed, M.; Iqbal, S.; Alhujaily, A.; Althobiti, R. A.; Alzahrani, E.; et al. Nanotheranostic fabrication of iron oxide for rapid photocatalytic degradation of organic dyes and antifungal potential. *J. Saudi Chem. Soc.* **2023**, *27* (5), 101689.

(32) Suppiah, D. D.; Julkapli, N. M.; Sagadevan, S.; Johan, M. R. Eco-friendly green synthesis approach and evaluation of environmental and biological applications of Iron oxide nanoparticles. *Inorg. Chem. Commun.* **2023**, *152*, 110700.

(33) Russo, M.; Iervolino, G.; Vaiano, V. W-doped zno photocatalyst for the degradation of glyphosate in aqueous solution. *Catalysts* **2021**, *11* (2), 234.

(34) Huo, R.; Yang, X.-L.; Liu, Y.-Q.; Xu, Y.-H. Visible-light photocatalytic degradation of glyphosate over BiVO4 prepared by different co-precipitation methods. *Mater. Res. Bull.* **2017**, *88*, 56−61.

(35) Nadi, A.; Boyer, D.; Charbonnel, N.; Boukhriss, A.; Forestier, C.; Gmouh, S. Immobilisation of bacteria onto magnetic nanoparticles for the decolorisation and degradation of azo dyes. *IET Nanobiotechnol.* **2019**, *13* (2), 144−149.

(36) Slavin, Y. N.; Asnis, J.; Hńfeli, U. O.; Bach, H. Metal nanoparticles: understanding the mechanisms behind antibacterial activity. *J. Nanobiotechnol.* **2017**, *15*, 65.

(37) Bhat, S. A.; Zafar, F.; Mondal, A. H.; Kareem, A.; Mirza, A. U.; Khan, S.; Mohammad, A.; Haq, Q. M. R.; Nishat, N. Photocatalytic degradation of carcinogenic Congo red dye in aqueous solution, antioxidant activity and bactericidal effect of NiO nanoparticles. *J. Iran. Chem. Soc.* **2020**, *17* (1), 215−227.

(38) Alshabanat, M. N.; Al-Anazy, M. M. An experimental study of photocatalytic degradation of congo red using polymer nano-composite films. *J. Chem.* **2018**, *2018*, 1−8.

(39) Erdemoğlu, S.; Aksu, S. K.; Sayılkan, F.; İzgi, B.; Asiltürk, M.; Sayılkan, H.; Frimmel, F.; Güçer, Ş. Photocatalytic degradation of Congo Red by hydrothermally synthesized nanocrystalline TiO2 and identification of degradation products by LC-MS. *J. Hazard. Mater.* **2008**, *155* (3), 469−476.

(40) Venkatachalam, N.; Palanichamy, M.; Murugesan, V. Sol-gel preparation and characterization of alkaline earth metal doped nano TiO2: Efficient photocatalytic degradation of 4-chlorophenol. *J. Mol. Catal. A: Chem.* **2007**, *273* (1−2), 177−185.

(41) Daneshvar, N.; Rabbani, M.; Modirshahla, N.; Behnajady, M. Kinetic modeling of photocatalytic degradation of Acid Red 27 in UV/TiO2 process. *J. Photochem. Photobiol., A* **2004**, *168* (1−2), 39−45.

(42) Pachapurkar, D.; Bell, L. N. Kinetics of thiamin degradation in solutions under ambient storage conditions. *J. Food Sci.* **2005**, *70* (7), c423.

(43) Wu, L.; Van Hoof, A. J.; Dzade, N. Y.; Gao, L.; Richard, M.-I.; Friedrich, H.; De Leeuw, N. H.; Hensen, E. J.; Hofmann, J. P. Enhancing the electrocatalytic activity of 2H-WS 2 for hydrogen evolution via defect engineering. *Phys. Chem. Chem. Phys.* **2019**, *21* (11), 6071−6079.

(44) Patil, S.; Deshmukh, S.; More, K.; Shevale, V.; Mullani, S.; Dhodamani, A.; Delekar, S. Sulfated TiO2/WO3 nanocomposite: An efficient photocatalyst for degradation of Congo red and methyl red dyes under visible light irradiation. *Mater. Chem. Phys.* **2019**, *225*, 247−255.

(45) Makvandi, P.; Wang, C. y.; Zare, E. N.; Borzacchiello, A.; Niu, L. n.; Tay, F. R. Metal-based nanomaterials in biomedical applications: Antimicrobial activity and cytotoxicity aspects. *Adv. Funct. Mater.* **2020**, *30*, 1910021.

(46) Ouyang, J.; Zhao, Z.; Suib, S. L.; Yang, H. Degradation of Congo Red dye by a Fe2O3@ CeO2-ZrO2/Palygorskite composite catalyst: synergetic effects of Fe2O3. *J. Colloid Interface Sci.* **2019**, *539*, 135−145.

(47) Taghavi Fardood, S.; Moradnia, F.; Moradi, S.; Forootan, R.; Yekke Zare, F.; Heidari, M. Eco-friendly synthesis and character-ization of α-Fe2O3 nanoparticles and study of their photocatalytic activity for degradation of Congo red dye. *Nanochem. Res.* **2019**, *4* (2), 140−147.

(48) Zhang, Y. J.; Liu, L. C.; Ni, L. L.; Wang, B. L. A facile and low-cost synthesis of granulated blast furnace slag-based cementitious material coupled with Fe2O3 catalyst for treatment of dye wastewater. *Appl. Catal., B* **2013**, *138−139*, 9−16.

(49) Ahmed, A.; Usman, M.; Yu, B.; Shen, Y.; Cong, H. Sustainable fabrication of hematite (α-Fe2O3) nanoparticles using biomolecules of Punica granatum seed extract for unconventional solar-light-driven photocatalytic remediation of organic dyes. *J. Mol. Liq.* **2021**, *339*, 116729.

(50) Sajid, M. M.; Shad, N. A.; Javed, Y.; Khan, S. B.; Zhang, Z.; Amin, N.; Zhai, H. Preparation and characterization of Vanadium pentoxide (V2O5) for photocatalytic degradation of monoazo and diazo dyes. *Surf. Interfaces* **2020**, *19*, 100502.

(51) Zhang, W.; Lan, Y.; Ma, M.; Chai, S.; Zuo, Q.; Kim, K.-H.; Gao, Y. A novel chitosan-vanadium-titanium-magnetite composite as a superior adsorbent for organic dyes in wastewater. *Environ. Int.* **2020**, *142*, 105798.

(52) Ullah, I.; Haider, A.; Khalid, N.; Ali, S.; Ahmed, S.; Khan, Y.; Ahmed, N.; Zubair, M. Tuning the band gap of TiO2 by tungsten doping for efficient UV and visible photodegradation of Congo red dye. *Spectrochim. Acta, Part A* **2018**, *204*, 150−157.

(53) Tien, T.-M.; Chung, Y.-J.; Huang, C.-T.; Chen, E. L. Fabrication of WS2/WSe2 Z-Scheme Nano-Heterostructure for Efficient Photocatalytic Hydrogen Production and Removal of Congo Red under Visible Light. *Catalysts* **2022**, *12* (8), 852.

(54) Oztekin, R.; Sponza, D. T. The Ionic Liquid-Assisted Synthesis of a Novel Polyaniline/Graphitic Carbon Nitride/Zinc Tungstate (PANI/gC 3N4/ZnWO4) Ternary Nanocomposite: The Usage a Easy Double Electron Transfer Photocatalyst for Glyphosate Photo-catalytic Degradation Process. *Clin. Interv. Clin. Trials* **2023**, *1*, 1.